Energetic Storm Particle Events in CME-driven Shocks

P. Mäkelä,[1,2] N. Gopalswamy,[2] S. Akiyama,[1,2] H. Xie,[1,2] and S. Yashiro[1,2]

S. Akiyama, The Catholic University of America, 620 Michigan Avenue N.E., Washington, DC 20064, USA. (sachiko.akiyama@nasa.gov)

N. Gopalswamy, NASA Goddard Space Flight Center, 8800 Greenbelt Road, Greenbelt, MD 20771, USA. (nat.gopalswamy@nasa.gov)

P. Mäkelä, The Catholic University of America, 620 Michigan Avenue N.E., Washington, DC 20064, USA. (pertti.makela@nasa.gov)

H. Xie, The Catholic University of America, 620 Michigan Avenue N.E., Washington, DC 20064, USA. (hong.xie@nasa.gov)

S. Yashiro, The Catholic University of America, 620 Michigan Avenue N.E., Washington, DC 20064, USA. (seiji.yashiro@nasa.gov)

[1]The Catholic University of America,

Washington, DC, USA.

[2]NASA Goddard Space Flight Center,

Greenbelt, MD, USA.

Abstract. We investigate the variability in the occurrence of energetic storm particle (ESP) events associated with shocks driven by coronal mass ejections (CMEs). The interplanetary shocks were detected during the period from 1996 to 2006. First we analyze the CME properties near the Sun. The CMEs with an ESP-producing shock are faster ($\langle V_{CME} \rangle = 1088$ km/s) than those driving shocks without an ESP event ($\langle V_{CME} \rangle = 771$ km/s) and have a larger fraction of halo CMEs (67% vs. 38%). The Alfvénic Mach numbers of shocks with an ESP event are on average 1.6 times higher than those of shocks without. We also contrast the ESP event properties and frequency in shocks with and without a type II radio burst by dividing the shocks into radio-loud (RL) and radio-quiet (RQ) shocks, respectively. The shocks seem to be organized into a decreasing sequence by the energy content of the CMEs: RL shocks with an ESP event are driven by the most energetic CMEs, followed by RL shocks without an ESP event, then RQ shocks with and without an ESP event. The ESP events occur more often in RL shocks than in RQ shocks: 52% of RL shocks and only ∼32% of RQ shocks produced an ESP event at proton energies above 1.8 MeV; in the keV energy range the ESP frequencies are 80% and 65%, respectively. Electron ESP events were detected in 19% of RQ shocks and 39% of RL shocks. In addition we find that (1) ESP events in RQ shocks are less intense than those in RL shocks; (2) RQ shocks with ESP events are predominately quasi-perpendicular shocks; and (3) their solar sources are located slightly to the east of the central meridian; (4) ESP event sizes show a modest positive correlation with the CME and shock speeds.

The observation that RL shocks tend to produce more frequently ESP events with larger particle flux increases than RQ shocks, emphasizes the importance of type II bursts in identifying solar events prone to producing high particle fluxes in the near-Earth space. However the trend is not definitive. If there is no type II emission, an ESP event is less likely but not absent. The variability in the probability and size of ESP events most likely reflects differences in the shock formation in the low corona and changes in the properties of the shocks as they propagate through interplanetary space, and the escape efficiency of accelerated particles from the shock front.

1. Introduction

Enhancements of energetic ions and electrons observed during an interplanetary (IP) shock passage are called energetic storm particle (ESP) events [Bryant et al., 1962]. They indicate local particle acceleration by the passing shock front. The time profiles of the ESP events are observed to vary from event to event. Particle intensities can show either gradual changes, i.e. increasing slowly before peaking near the time of shock passage followed by a slow decrease, or more rapid changes, i.e. short-duration spikes or step-like increases [see e.g., Sarris and Van Allen, 1974; Tsurutani and Lin, 1985; Kallenrode, 1995; Lario et al., 2003, 2005; Cohen, 2006]. However, most commonly ESP events appear more irregular, and their occurrence is energy dependent [Lario et al., 2005]. The time profile and acceleration efficiency of particles depend on the shock normal angle θ_{Bn}, i.e. on the angle between the magnetic field direction ($\mathbf{B}$) and the shock normal direction ($\mathbf{n}$): spike-like events are observed during quasi-perpendicular shocks and events with more slowly varying intensities with quasi-parallel shocks. The ion acceleration rate is faster in perpendicular shocks than in parallel shocks, and therefore the attained maximum energy of particles is higher in perpendicular shocks [Jokipii, 1987; Giacalone, 2005]. Electron acceleration efficiency also depends on the shock normal angle θ_{Bn} [e.g., Krauss-Varban et al., 1989, 1991]. In general, differences in the features of the intensity-time profiles and also in the properties of shock fronts have been observed when the same ESP event and shock has been observed by different spacecraft [e.g., Neugebauer et al., 2005, 2006].

Recent studies of ESP events have mainly focused on the local plasma, magnetic field and particle observations near 1 AU. Both Lario et al. [2005] and Ho et al. [2008] studied

the properties of 191 fast forward shocks and the associated ESP events observed by the ACE spacecraft from February 1998 to October 2003. Lario et al. [2005] note that stronger and faster shocks more likely influence local particle fluxes, but they do not find any strong correlations between shock parameters and the ESP event characteristics. Ho et al. [2008] report that 64% and 31% of the shocks exhibited an ion flux enhancement in the 47–68 keV and 1.9–4.8 MeV range respectively. Only 20% of shocks showed an electron ESP events in the 38–53 keV energy channel. Huttunen-Heikinmaa and Valtonen [2009] studied ESP events above 1.5 MeV associated with fast forward shocks that occurred between May 1996 and April 2003 using the SOHO/ERNE data. However, they did not consider the shock driver, so their data set also includes shocks associated with corotating interaction regions (CIRs). They found that 46% of fast forward shocks did not show any signs of an ESP event. In general there is a poor association between IP shocks and ESP events.

Type II radio bursts provide an alternative signature of particle acceleration in traveling transient shocks. Electrons accelerated in CME-driven shocks can generate type II radio emission observed in dynamic radio spectra as an intermittent or continuous lane that slowly decrease in frequency. Emission occurs most intensely around the fundamental and/or second harmonic of local plasma frequency [see e.g., Nelson & Melrose, 1985]. The observed decrease in frequency is due to a decrease in the plasma density with the distance from the Sun. The highest-frequency emission at metric wavelengths originate from shocks in the low corona, followed by emission at decameter-hectometric (DH) and kilometric wavelengths as the shock travels outwards. However, some fast and wide CMEs that are expected to be energetic enough to drive shocks, are not associated with type II

radio bursts [e.g., Gopalswamy et al., 2008b]. Gopalswamy et al. [2010a] reported that a large fraction (34%) of IP CME-driven shocks could not be associated with observable type II radio emission. A fast-mode shock should form in front of the CME when the CME speed relative to the ambient medium exceeds the local Alfvén speed. Therefore variations in the CME speed [for CME acceleration or deceleration see e.g., Yashiro et al., 2004; Gopalswamy, 2006] and in the Alfvén speed [see e.g., Gopalswamy et al, 2001; Mann et al., 2003] in the corona and IP space can affect particle acceleration in the CME-driven shocks.

Both type II radio bursts and ESP events thus demonstrate the ability of shocks to accelerate particles. In the largest ESP events, the particle fluxes can reach the highest levels observed near Earth during a solar particle event. Therefore, ESP events constitute a significant phenomenon for space weather applications, and hence studies of the ESP event occurrence rate and association with solar and IP phenomena can benefit space weather research. In this study we first investigate if the CME properties make a difference in the ESP events produced by their shocks. Then we concentrate on the question how the ESP events and the type II bursts produced by the same shock relate to each other. The relevance of the selected focus on relations between ESP events and type II bursts is further underpinned by known correlations between type II bursts and solar energetic particle (SEP) acceleration: [Gopalswamy et al., 2002] found all large SEP events in their study to be associated with DH type IIs ; Cliver et al. [2004] found that 82% of a different set of $\sim$ 20 MeV SEP events are associated with metric and 63% with DH type IIs, and the overall association is even higher, 90%, for the DH type IIs in the western hemisphere accompanied with a metric type II burst. To our knowledge correlations between type II

radio emission and ESP events have not been studied before using a statistically significant set of CME-driven shocks. A full description of the characteristics of CMEs and shocks, including their association with type II radio emission, and the list of events studied in this paper can be found in Gopalswamy et al. [2010a]. Properties of RQ and RL CMEs are also discussed in Gopalswamy et al. [2008b]. The study of Gopalswamy et al. [2008a] concentrated on SEPs while we focus on ESP events.

2. Observations

Gopalswamy et al. [2010a] compiled a list of 230 CME-driven shocks observed at 1 AU by one or more of the Advanced Composition Explorer (ACE), the Solar and Heliospheric Observatory (SOHO), and the Wind spacecraft during 1996–2006. For each shock they identified the source region at the Sun and found the associated CME driving the shock. They also searched for associated type II emission during each event in the metric-to-kilometric wavelength range and verified the in-situ ejecta signatures in the plasma and magnetic field measurements at 1 AU. Based on the existence of an associated type II burst, they divided shocks accordingly into radio-loud (RL) and radio-quiet (RQ) events. Two shocks lacked conclusive radio measurements and are not included in the RQ or RL shocks. In the analysis they used data both from spacecraft (SOHO, ACE, Wind, GOES) and from the ground-based observatories. As the full details of the data sources and analysis utilized in compiling of the shock list are explained in the paper by Gopalswamy et al. [2010a], we will not repeat them here.

Using the shock list by Gopalswamy et al. [2010a] we searched for associated ESP events in the IP proton and electron flux during the shock passages. The particle observations were provided by the Electron, Proton, and Alpha Monitor (EPAM) [Gold et al., 1998]

on board ACE and Energetic and Relativistic Nuclei and Electron (ERNE) [Torsti et al., 1995] experiment on board SOHO. We made use of ion measurements by LEMS120 of EPAM in the 66–4750 keV range and ERNE measurements in 1.8–50.1 MeV range. As the ACE spacecraft was launched in 1997, we excluded a total of 8 pre-ACE shocks and one other shock due to data gap while searching the low-energy proton and electron flux. In the survey of high-energy protons flux, we excluded only 1 event since SOHO/ERNE data are available in this energy range. Based on the highest energy channel in which the ESP event was clearly observable, we classified the events roughly into two categories: enhancements in the keV and in the MeV ranges, i.e., events observed below and above ≈ 1.8 MeV. In addition to proton intensities, we searched for ESP events in the electron measurements made by ACE/EPAM.

We estimated the size of the ESP event in the two EPAM/LEMS120 0.114–0.190 keV and 1.89–4.75 MeV energy channels and in the EPAM/DE30 38-53 keV electron channel. We define the size of the ESP increase as the peak intensity subtracted by the background intensity. The background intensity, either due to a quiet-time particle flux or possibly an ongoing SEP event, was estimated during a period before the start of the ESP event. In the case of slowly increasing ESP events, we allowed at most 36 hours interval between the end of background period and the time of the shock passage. We assumed that the background intensity follows an exponential decay with time. One should note that during high background intensities it is possible that smaller ESP events could not be detected. All ESP peaks are at least 15% above the estimated background and within 12 hours of the shock passage. An example of the size estimation of the ESP event is shown in Figure 1. The vertical solid lines show the estimated size of the flux increase observed by

ACE/EPAM in the 0.114-0.190 MeV and 1.89–4.75 MeV range during the 10 July 2000 shock.

3. CME Properties and Shock Mach Numbers

In this section we describe briefly the properties of the associated CMEs near the Sun and look at also the shock Mach numbers at 1 AU. One could expect the possible differences in the dynamic properties of CMEs to be more pronounced near the Sun than at 1 AU, because propagating CMEs decelerate/accelerate towards the solar wind speed due to interactions with the surrounding plasma [see e.g., Yashiro et al., 2004; Gopalswamy, 2006].

3.1. CMEs driving Shocks with and without an ESP Event

First we looked at the CME properties in two separate groups: CMEs driving shocks with and without an ESP event. Figure 2 shows the distributions of the CME speed (V_{CME}), width (W_{CME}), and acceleration (a_{CME}) as observed by SOHO/LASCO. The top row panels show distributions for CMEs with an ESP event either in the keV or MeV range or both. The bottom row panels show the data for CMEs without any observable ESP event. Clearly the CMEs associated with an ESP event are faster (average speed 1088 km/s, Fig 2a) than those without (average speed 771 km/s, Fig 2d). The average widths of non-halo CMEs in both categories are similar (155° vs 159°), but there is a significant difference in the fraction of halo CMEs. About 67% of CMEs with an ESP event are halos, compared to 38% of those without. As the fraction of halo CMEs is known to be a good proxy to how energetic the CME population is on average [see e.g.,

Gopalswamy et al., 2010b], this result indicates that the ESP events are associated with more energetic CMEs as expected.

3.2. Radio-loud and Radio-quiet Shocks

Next we divided the two CME categories with and without an ESP event further into two subgroups: CMEs driving RL and RQ shocks. In Figures 3 and 4 we have plotted the distributions as in Figure 2 for RL and RQ shocks with and without an ESP event. For RL shocks with and without an ESP event, the largest differences are in the fraction of halo CMEs and CME acceleration. The halo CMEs are 1.75 times more frequent in RL shocks with an ESP event than in those without. The average CME deceleration for RL shock without an ESP event (-6.3 m/s^2) is twice that for RL shock with an ESP event (-3.1 m/s^2). Also the average CME speed is higher for RL shocks with an ESP event. The results indicate that CMEs associated with RL shocks without an ESP event are less energetic and experience larger deceleration already near the Sun. The larger number of non-halo CMEs means also that most likely in those events only the weaker flank of the shock is arriving at Earth. This naturally explains the observed lack of local particle acceleration at the shocks as they arrive at 1 AU. However, the differences in CME characteristics for RQ shocks with and without an ESP event are less pronounced. The observed average accelerations are comparable, and the halo CME ratio and average CME speed are only marginally higher for CMEs driving shocks with an ESP event. This could suggests that the changes affecting particle acceleration efficiency occur in the later phase of the shock transit when the RQ shock has propagated beyond the LASCO field of view. In the broader view, the CME dynamic characteristics appear to structure the events into a distinct sequence: RL shock with an ESP event are driven by the most

energetic CMEs, followed by RL shocks without an ESP event, RQ shocks with an ESP event and finally RQ shocks without an ESP event, all driven by successively less energetic CMEs.

3.3. Mach Numbers of Shocks with and without an ESP Event

In Figure 5 we have plotted the distributions of the Alfvénic Mach numbers at 1 AU obtained from Gopalswamy et al. [2010a]. In the plots we have excluded Mach numbers greater than 10, because most likely those very high values are not real. It is not always possible reliably estimate instantaneous plasma parameters in the vicinity of the shock under disturbed conditions, and these uncertain estimates can result in errors in calculated Mach numbers. One should also note that Mach numbers are based on single-point plasma measurements, whereas particles encounter multiple parts of the shock front during their acceleration. The plot for all shocks shown in Fig. 5a clearly suggests a bimodal distribution of Alfvénic Mach numbers with peaks at ~ 1.2 and ~ 2.5. The average value of the Mach number for all shocks is ~ 3.13 and it is given in the plot together with the standard deviation (STD) and the median value. In the other two plots of Figure 5 we have plotted the Mach numbers divided into two categories like we did for CMEs in Fig. 2, i.e. shocks with (Fig. 5b) and without (Fig. 5c) an ESP event. This division clearly separates the two-peak distribution into its components. The average Mach number for shocks with an ESP (Fig 5a) is $\sim$ 3.46, about 1.6 times the value of $\sim$ 2.22 obtained for shocks without an ESP event (Fig 5c). If we restrict further the Mach number range to values less or equal to 5 in order to better exclude the more uncertain tail of the distributions, we obtain the respective average and median Mach numbers: 2.49 and 2.39 for all shocks; 2.67 and 2.49 for shocks with an ESP event; 2.02 and 1.90 for those without an ESP event.

The differences become less substantial, but reflect better the true peak positions. The Mach number ranges of the two distributions do overlap each other, indicating that Mach number alone cannot describe the particle acceleration efficiency of the shocks. However, it is clear that higher Mach number shocks accelerate particles more readily.

4. Association between Type II Bursts and ESP Events

Next we examined the occurrence of ESP events in association with the selected 82 RQ and 146 RL CME-driven shocks observed during 1996–2006. There were data gaps during 9 shocks in the observations of keV particles and during one shock in the MeV range particle observations. We found that $\sim 65\%$ (50 events out of 77) and $\sim 32\%$ (27 events out of 82) of RQ shocks had an ESP event in the keV and MeV range, respectively (Table 1). As mentioned, the difference in the total numbers of RQ shocks is due to the difference in the coverage of particle observations in the keV and MeV range. In the case of RL shocks, the corresponding fractions of ESP events were higher: $\sim 80\%$ (114 events out of 142) and $\sim 52\%$ (75 events out of 145), respectively. Therefore, the RL shocks are far more likely to have observable increase of proton flux at 1 AU than the RQ shocks. There are more ESP events in the lower energy range. We observed a total of 168 ESP events and 122 events of those in both energy ranges. For electrons, we found that 19% (15 out of 77) of RQ shocks and 39% (55 out of 142) of RL shocks were associated with an ESP event in the 38–53 keV energy range. We excluded 9 shocks with data gaps in electron observations. It is well-known that electron enhancements are observed less frequently than ion enhancements during IP shocks [e.g., Tsurutani and Lin, 1985]. The selection of ESP events was made based on time-intensity profiles. It is evident that there is some ambiguity in the selection of the events, as the time-profiles of ESP events varied

widely. In the case of quasi-parallel shocks, the increase can be relatively small and slowly evolving compared to the shock spike events that are associated with quasi-perpendicular shocks. As we discuss in the next section, the average size of ESP events associated with the RQ shocks are also considerably smaller than those associated with the RL shocks.

5. ESP Event Sizes

In Figure 6 we have plotted the ESP event sizes as a function of shock (panels on the left) and CME speeds (panels on the right). Only RL shocks have associated ESP events at high CME and shock speeds. The shock and CME speeds of RQ shocks with an ESP event are below ~ 700 km s^{-1} and ~ 1000 km s^{-1}, respectively (vertical dotted lines in the bottom panels). In addition, CME speeds clearly separate the RL and RQ events better than the shock speeds do, as explained in Gopalswamy et al. [2010a]. On average, the ESP sizes of RL shocks are higher than those of RQ shocks: The average event size for the keV- and MeV-range protons during RQ shocks were 2.4×10^4 cm^{-2} s^{-1} st^{-1} MeV^{-1} and 4.0×10^1 cm^{-2} s^{-1} st^{-1} MeV^{-1}, respectively. The ESP event size for RL shocks were 1.2×10^5 cm^{-2} s^{-1} st^{-1} MeV^{-1} and 2.4×10^3 cm^{-2} s^{-1} st^{-1} MeV^{-1}. In the low-energy channel the spread of enhancements is nearly similar for both RQ and RL shocks. In the high-energy channel, the ESP event sizes of RQ shocks are below 3×10^2 cm^{-2} s^{-1} sr^{-1} MeV^{-1} (marked by the horizontal dotted line), and the maximum ESP event size of RL shocks is ≈ 100 times higher.

Figure 7 shows the size of electron ESP events in the 38-53 keV energy range as a function of shock and CME speeds. The difference in the electron event size between RQ and RL events is even more significant than that in proton events. The average size of the electron ESP event for RQ shocks was 1.7×10^4 cm^{-2} s^{-1} st^{-1} MeV^{-1} and for RL

shocks 9.3×10^5 cm^{-2} s^{-1} st^{-1} MeV^{-1}. However, the electron enhancements are observed less frequently than the proton enhancements during the shock passage.

We also looked at the correlations between the size of ESP events and the CME and shock speeds. To do that we calculated the rank correlation coefficients, ρ, and error probabilities, $P(e)$, for RQ, RL, and all shocks as listed in Table 2. Most of the correlations are modest for both RQ and RL shocks. The correlation coefficients vary between 0.76 and 0.26. The low error probabilities indicate that the correlations are real. All correlation coefficients for RL shocks are higher than the corresponding ones for RQ shocks, except for the correlation of RL event size with the CME speed in the MeV range. The rank correlations when all shocks are included fall between 0.70 and 0.59 with small error probabilities. Electron observations reveal a general trend similar to the proton observations, but we did not conduct a more detailed analysis as there are fewer shocks associated with electron enhancements (small sample).

6. Shock Normal Angles

In Figure 8 we have plotted the local shock normal angle θ_{Bn} as a function of the source longitude (see also Table 1). The shock normal angles are either from the Kasper shock database or calculated with SDAT program. For 9 RQ and 16 RL shocks θ_{Bn} calculations were not available. We have divided shocks into three categories, i.e. quasi-parallel ($\theta_{Bn} = 0°$–$30°$), oblique ($\theta_{Bn} = 30°$–$60°$), and quasi-perpendicular ($\theta_{Bn} = 60°$–$90°$). There is a difference in the occurrence frequency between RQ and RL shocks with and without an ESP event. The quasi-perpendicular shocks appear to be more dominating in the RQ shocks with an ESP event. The fraction of quasi-perpendicular RQ shocks is 65% (15 out of 23) and 48% (24 out of 50) for shocks with and without an ESP event.

The same fraction for RL shocks is 55% (37 out of 67) and 44% (27 out of 62) for shocks with and without an ESP event, respectively. The larger fraction of ESP events in RQ quasi-perpendicular shocks is probably related to faster particle acceleration rate in quasi-perpendicular shocks, which enables particles to reach higher energies [e.g., Jokipii, 1987; Decker, 1988; Webb et al., 1995]. One should note that observations of θ_{Bn} are point measurements, which are affected by local irregularities of shock fronts. This probably explains why θ_{Bn} does not show any clear dependence on the source longitude that one might expect assuming smooth shock front and nominal Parker spiral of interplanetary magnetic field. One should further note that particles interact with large areas of shock front during their acceleration.

We have plotted the size of electron ESP events as a function of shock normal angle in Figure 9. Again, the dotted lines are plotted to emphasize that the electron enhancements associated with RQ shocks are very small in size ($J < 10^5$ cm^{-2} s^{-1} st^{-1} MeV^{-1}) and the shock normal angles in all RQ events are larger than 50°. For comparison, 70% (37 out of 53) of RQ shocks without an electron ESP event had $\geq 50°$. The shock normal angle of RL shocks and the size of the associated electron increases both have a broader distribution than those of the RQ shocks. The large shock angles of RQ shocks and RL shocks with high electron intensity are consistent with the theoretical prediction that electrons are more efficiently accelerated by quasi-perpendicular shocks.

7. Solar Source Distributions

In order to better see the difference between the solar source locations of RQ and RL shocks with and without an ESP event, we have plotted separately the source longitudinal (left) and latitudinal (right) distributions in Figures 10 and 11. The left-hand panels in

Figure 10 clearly show that on average the RQ shocks with an ESP event (blue line) originate from more eastern source locations than shocks without an ESP event. We believe that this shift in source longitudes reflects the east-west asymmetry in the relative size of ESP events. It was first reported by Sarris et al. [1984] in their study of ESP events observed by IMP-7 and 8 spacecraft [see also Sarris et al., 1985; Meyer et al., 1993]. They attributed the asymmetry to the change of the average shock normal angles from quasi-perpendicular in the western flank to quasi-parallel in the eastern flank. Therefore, the asymmetry indicates the difference in the efficiency of particle acceleration processes in quasi-parallel and quasi-perpendicular shocks. For RQ CMEs launched from east of the central meridian, an observer at 1 AU intercepts the western flank of the shock nose and hence is more likely to observe an ESP event, which on average has a large relative size. Consistently, Cane [1988] observed that IP shocks originating east of central median have the highest average shock strength. Because CMEs associated with RQ shocks are also less energetic than those with RL shocks [Gopalswamy et al., 2010a], their overall ability to accelerate particles is reduced. Therefore, the smaller ESP events will be more likely near our detection limit. Also the longitudinal extent of the efficient particle acceleration region, i.e. the shock nose region, will be narrower. The distributions of RL source locations do not show a similar longitudinal shift. Both flanks are likely to be able to produce ESP events well above the detection limit. The latitudinal distributions of sources shown in the right-hand panels of Figures 10 and 11 do not reveal any major differences between the shocks with and without an ESP event in either energy range. The source latitudes are confined to $\pm 30^{\circ}$ suggesting that the shock-driving CMEs originate in the active region belt [Gopalswamy, 2010].

8. Discussion

Using a list of CME-driven shocks observed at 1 AU and their association with type II radio bursts compiled by Gopalswamy et al. [2010a], we have surveyed ESP events during these shocks, contrasting between shocks that did and did not produce type II bursts. Type II radio bursts are related to shock acceleration of electrons near the Sun and the IP space. Therefore, the type II bursts provide information about particle acceleration by shocks closer to the Sun, whereas the ESP events tell about local particle acceleration when the shock reaches 1 AU. As proton intensities during ESP events at 1 AU can reach very high levels, understanding the factors affecting the occurrence and properties of ESP events is relevant for space weather applications and for space weather research in general.

8.1. CME Characteristics

In general, CMEs driving shocks with an ESP event are more energetic, i.e., the average speed and also the fraction of halo CMEs are higher than those for CMEs driving shocks without an ESP event. The average acceleration observed in the LASCO field of view is equal. A further division into RL and RQ shocks reveals that the CMEs driving RL shocks without an ESP event are less energetic (lower average speed and fraction of halo CMEs) and have the highest average deceleration near the Sun. For CMEs driving RQ shocks the differences in the CME characteristics are less significant. The average speed and halo CME ratio are only slightly higher for shocks with an ESP event than for shocks without an ESP event. The average accelerations are comparable. The difference in shock particle acceleration processes probably evolves later during the RQ shock transit to 1 AU. However, when compared to CMEs driving RL shocks, they are considerably slower, accelerate instead of decelerating, and have fewer halo CMEs. The energy of the

associated CME seems to organize the events to a natural sequence: CMEs driving RL shocks with an ESP event are the most energetic ones, followed by CMEs driving RL shocks without an ESP event and CMEs driving RQ shocks with an ESP event, while CMEs diving RQ shocks without an ESP event are the least energetic ones.

8.2. Alfvénic Mach Numbers

Alfvévic Mach numbers are widely used to describe the strength of shock fronts. The Mach number distribution of the general shock population (Fig. 5a) shows two peaks at $\sim$ 1.2 and $\sim$ 2.5 indicating that the general shock population consists of two shock populations. Figures 5b and c suggest that the existence or lack of an associated ESP event could characterize these two components. The average Mach numbers of these two populations are 3.46 and 2.22, respectively. These values are comparable with the average Mach numbers reported by Gopalswamy et al. [2010a] to be 3.4 for RL shocks and 2.6 for RQ shocks. Gopalswamy et al. [2010a] also discuss extensively about first critical Mach number [see Edmiston and Kennel, 1984] , which they estimate to be 1–2.3 at 1 AU, and its significance for electron shock acceleration and hence for type II radio emission. They suggest that RQ shocks are subcritical, i.e. have Mach numbers less than the critical Mach number, whereas RL shocks are supercritical. Based on the average Mach numbers found in our study, a similar distinction can be made between shocks with and without an ESP event. This result indicates a relationship between type II emission and ESP events, which we studied next in more detail.

8.3. ESP Event Frequency in RL and RQ Shocks

When ESP events are considered separately in RL and RQ shocks, the ESP rates differ significantly. Our study shows that RL shocks have a much higher fraction of ESP events ($\sim$ 80% and $\sim$ 52% respectively in the keV and MeV energy range) than RQ shocks ($\sim$ 65% and $\sim$ 32% correspondingly). We find a similar difference in the frequency of keV electron ESP events between RL ($\sim$ 39%) and RQ ($\sim$ 20%) shocks. Noteworthy is also that some RQ shocks are associated with an ESP event at 1 AU. This reflects the evolution of the shock properties as shocks propagate towards Earth. In an earlier survey, Kallenrode [1996] studied shocks observed by the two Helios spacecraft between 1974 and 1985, and their association with increases of near-Sun accelerated particle flux (solar component) and of shock-associated particle flux (IP component). Kallenrode [1996] reported that acceleration of MeV particles near the Sun does not correlate with the IP acceleration of MeV particles. This resembles the difference in the ESP event frequency between RQ and RL shocks we found. Even though ESP events occur considerably more frequently in RL shocks, there is no clear-cut relation between type II radio emission (solar component) and ESP events at 1 AU (IP component). Of course, there is no one-to-one correspondence between SEP events and type II bursts. However, strong correlations exist depending on the wavelength of the type II burst and size of the SEP event. Gopalswamy et al. [2002] found that all large SEP events in their study were associated with DH type IIs. Cliver et al. [2004] found the overall percentage association of a different set of SEP events to be 82% with metric, 63% with DH type IIs, and 90% for the DH type IIs in the western hemisphere accompanied with a metric type II burst.

Comparisons with earlier studies show that the overall fraction of shocks with ESP increases in our study is similar to previous studies. About 75% and 45% of all the CME-driven shocks in our survey have an ESP event in the keV and MeV range, respectively, and about 33% have an electron ESP event. The RL shocks have higher rate of ESP events than the general population studied by Ho et al. [2008], indicating the effectiveness of RL shocks in accelerating energetic particles.

8.4. Size of ESP Events and Correlation with CME and Shock Properties

Again when we study the size of the ESP event in the 0.114–0.190 keV and 1.89–4.75 MeV proton channels separately in RL and RQ shocks, we find a difference. On average the RL shocks are associated with larger ESP events than the RQ shocks. Same is true for electron ESP events. Considering space weather applications and the good correlation of RL shocks with large SEP events, this results emphasizes the significance of type II bursts in identifying solar events prone to produce higher particle fluxes in the near-Earth space. When we look at the correlation of the size of the ESP event size with the shock and CME speeds that are commonly used, we observe that the spread in the ESP event sizes is considerable, and the correlations are moderate at best. Previous studies of ESP event sizes in association with various shock parameters have resulted in similar moderate correlations [e.g., van Nes et al., 1984; Cane et al., 1990; Kallenrode, 1996]. However, we find that RL shocks show in 3 cases out of 4 (Table 2) a better correlation with the CME and shock speed than RQ shocks. As RQ CMEs are slower and less energetic than RL CMEs, it is possible that RQ CMEs are affected more by the ambient plasma environment during their propagation to 1 AU.

We also looked at the shock normal angle θ_{Bn} in RL and RQ shocks with and without an ESP event (Table 1). We find that a larger fraction (65%) of RQ shocks with an ESP event in the MeV range has the shock normal angle $\theta_{Bn} \geq 60^{\circ}$ compared to the RQ shocks without an ESP event (48%). The difference is slightly less pronounced in RL shocks. However, one must point out that shock normal angle evolves as CMEs expand outwards. Therefore, the shock normal angle observed at 1 AU does not necessarily describe well the conditions near the Sun. Another factor affecting θ_{Bn} measurements is its spatial variation along the shock surface due to the undulation of the shock front, which can result in different θ_{Bn} values observed by separate spacecraft [e.g., Neugebauer et al., 2005, 2006]. Particles in ESP events are accelerated over large areas of the shock front before detection. The variation of the θ_{Bn} along the shock front is probably important. The variation explains why the local θ_{Bn} does not depend on the source longitude even though the source locations of RQ shocks with and without an ESP event show a longitudinal dependence associated with global topology of the IP magnetic field and the shock. However, we believe that our statistical results are still valid, because differences in individual values observed by spacecraft at different locations do not imply a significant change in the distribution of observed values.

8.5. Source Locations at the Sun

We find a longitudinal shift between the source locations of RQ shocks with and without an ESP event at 1 AU. RQ shocks without an ESP event are more preferably launched from the region west of central meridian (see Figure 10). We believe that this longitudinal shift reflects observational bias in detection due to east-west asymmetry in relative ESP event size first observed by Sarris et al. [1984] when studying ESP events observed

by IMP-7 and 8 spacecraft [see also Sarris et al., 1985; Meyer et al., 1993]. They attribute the east-west asymmetry to the change of the average shock normal angles from quasi-perpendicular in the western flank to quasi-parallel in the eastern flank, and to the difference in particle acceleration processes in quasi-parallel and quasi-perpendicular shocks. Similar east-west asymmetry was reported in the average shock strengths by Cane [1988]. In general, the RQ and RL source distributions reflect the width of the shock front ahead of a propagating CME. Gopalswamy et al. [2010a] reported that RL CMEs and the associated shocks are faster, i.e. more energetic, than RQ CMEs and shocks. Faster CMEs are generally wider, so the wider RL shocks with a larger longitudinal separation between the solar source and the observer can still be detected at 1 AU. In a study of CME widths, Michalek et al. [2007] found that radio-loud CMEs are almost two times wider than radio-quiet CMEs [see also Gopalswamy et al., 2008b]. The source distribution of RQ and RL shocks differs considerably from that of RQ and RL fast and wide CMEs studied by Gopalswamy et al. [2008b]. They found that sources of RQ CMEs are located near the limbs, whereas for RL CMEs occur in center-west regions of the solar disk. They also suggest that the reduced visibility of the shock surface, together with the radio emission propagation and CME projection effects could explain the preponderance of limb CMEs among the RQ CMEs.

9. Conclusions

The energy content of the shock-driving CMEs, indicated by the CME speed and fraction of halo CMEs, seems to organize the events to a sequence where RL shocks with an ESP event are driven by the most energetic CMEs. The RL shocks without an ESP event are driven by slightly less energetic CMEs, followed by CMEs driving RQ shocks

with and without an ESP event in decreasing order of the CME energy. The distribution of Alfvénic Mach numbers for all shocks has two peaks. This bimodal distribution can be explained by two shock populations, where shocks with an ESP event have on average 1.6 times higher Mach numbers than shocks without. The ESP events associated with the RQ shocks are significantly less frequent and less intense than those associated with the RL shocks. Only ∼32% of RQ shocks is associated with an ESP event at energies above 1.8 MeV, compared to 52% of RL shocks. In the keV energy range the association rate is higher: 80% of RL shocks and 65% of RL shocks have an ESP event. ESP events in the electron flux are more infrequent that the in proton flux: 19% of RQ shocks and 39% of RL shocks have an electron ESP event. RQ shocks with an ESP event originate preferably from source regions east from the central meridian, whereas the RQ shocks without an ESP event have more western sources. The variability in the probability and size of the ESP events most likely reflects differences in the shock formation in the low corona and changes in the properties of the shocks as they propagate through IP space, and the escape efficiency of accelerated particles from the shock front. The production of type II bursts also involves additional steps of wave production and their conversion to radio waves following the acceleration of electrons. The implications of these results and the known good correlation of RL shocks with large SEP events for space weather forecasting is that they underpin the significance of type II bursts in identifying solar events producing high particle fluxes in the near-Earth space.

Acknowledgments. This research was supported by NASA grants NNX08AD60A and NNX10AL50A. SOHO is an international cooperation project between ESA and NASA.

References

Bryant, D. A., T. L. Cline, U. D. Desai, and F. B. McDonald (1962), Explorer 12 observations of solar cosmic rays and energetic storm particles after the solar flare of September 28, 1951, *J. Geophys. Res., 67*, 4983–5000, doi:10.1029/JZ067i013p04983

Cane, H. V., The Large-Scale Structure of Flare-Associated Interplanetary Shocks, *J. Geophys. Res., 93*, 1–6, doi:10.1029/JA093iA01p00001

Cane, H. V., T. T. von Rosenvinge, and R. E. McGuire (1990), Energetic particle observations at the HELIOS 1 spacecraft of shocks associated with coronal mass ejections, *J. Geophys. Res., 95*, 6575-6579, doi:10.1029/JA095iA05p06575

Cliver, E. W., S. W. Kahler, and D. V. Reames (2004), Coronal shocks and solar energetic proton events, *Astrophys. J., 605*, 902–910, doi:10.1086/382651

Cohen, C. M. S. (2006), Observations of Energetic Storm Particles: An Overview, in *Solar eruptions and energetic particles, Geophys. Monogr. Ser.*, vol. 165, edited by N. Gopalswamy, R. Mewaldt, and J. Torsti, pp. 275-282, AGU, Washington, D.C.

Decker, R. B. (1988), Computer modeling of test particle acceleration at oblique shocks, *Space Sci. Rev., 48*, 195–262, doi:10.1007/BF00226009

Edmiston, J. P. and C. F. Kennel, A parametric survey of the first critical Mach number for a fast MHD shock, *J. Plasma Phys., 32(3)*, 429–441, doi:10.1017/S002237780000218X

Giacalone, J. (2005), Particle acceleration at shocks moving through an rrregular magnetic field, *Astrophys. J., 624*, 765-772, doi:10.1086/429265

Gold, R. E., S. M. Krimigis, S. E. Hawkins, III, D. K. Haggerty, D. A. Lohr, E. Fiore, T. P. Armstrong, G. Holland, and L. J. Lanzerotti (1998), Electron, Proton, and Alphamonitor on the Advanced Composition Explorer spaceraft, *Space Sci. Rev., 86*, 541–562,

doi:10.1023/A:1005088115759

Gopalswamy, N. (2010), Large-scale solar eruptions, in *Heliophysical Processes, Astrophys. Space Sci. Proc.*, edited by N. Gopalswamy, S. S. Hasan, and A. Ambastha, pp. 53–71, Springer, Heidelberg, doi:10.1007/978-3-642-11341-3_4

Gopalswamy, N., A. Lara, M. L. Kaiser, and J.-L. Bougeret (2001), Near-Sun and near-Earth manifestations of solar eruptions, *J. Geophys. Res., 106*, 25261–25278, doi:10.1029/2000JA004025

Gopalswamy, N., S. Yashiro, G. Michałek, M. L. Kaiser, R. A. Howard, D. V. Reames, R. Leske, and T. von Rosenvinge, T. (2002), Interacting coronal mass ejections and solar energetic particles, *Astrophys. J., 572*, L103–L107, doi:10.1086/341601

Gopalswamy, N. (2006), Coronal mass ejections of solar cycle 23, *J. Astrophys. Astron., 27*, 243, doi:10.1007/BF02702527

Gopalswamy, N., S. Yashiro, S. Akiyama, P. Mäkelä, H. Xie, M. L. Kaiser, R. A. Howard, and J.-L. Bougeret (2008b), Coronal mass ejections, type II radio bursts, and solar energetic particle events in the SOHO era, *Ann. Geophys., 26*, 3033–3047, doi:10.5194/angeo-26-3033-2008

Gopalswamy, N., S. Yashiro, H. Xie, S. Akiyama, E. Aguilar-Rodriguez, M. L. Kaiser, R. A. Howard, and J.-L. Bougeret (2008a), Radio-quiet fast and wide coronal mass ejections, *Astrophys. J., 674*, 560–569, doi:10.1086/524765

Gopalswamy, N., H. Xie, P. Mäkelä, S. Akiyama, S. Yashiro, M. L. Kaiser, R. A. Howard, and J.-L. Bougeret (2010a), Interplanetary shocks lacking type II radio bursts, *Astrophys. J., 710*, 1111–1126, doi:10.1088/0004-637X/710/2/1111

Gopalswamy, N., S. Yashiro, G. Michalek, H. Xie, P. Mäkelä, A. Vourlidas, and R. A. Howard (2010b), The Catalog of Halo Coronal Mass Ejctions from SOHO, *Sun and Geosphere, 5(1)*, 7–16

Ho G. C., D. Lario, R. B. Decker, C. W. Smith, and Q. Hu, (2008), Transient shocks and associated energetic particle distributions observed by ACE during cycle 23, in *Particle Acceleration and Transport in the Heliosphere and Beyond, AIP Conf. Proc.*, vol. 1039, edited by G. Li, Q. Hu, O. Verkhoglyadova, G. P. Zank, R. P. Lin, and J. Luhmann, pp. 184–189, AIP, Melville, New York, doi:10.1063/1.2982443

Huttunen-Heikinmaa, K., and E. Valtonen (2009), Interplanetary fast forward shocks and energetic storm particle events above 1.5 MeV, *Ann. Geophys., 27*, 767–779, doi:10.5194/angeo-27-767-2009

Jokipii, J. R. (1987), Rate of energy gain and maximum energy in diffusive shock acceleration, *Astrophys. J., 313*, 842–846, doi:10.1086/165022

Kallenrode, M.-B. (1995), Particle acceleration at interplanetary shocks – observations at a few tens of keV vs some tens of MeV, *Adv. Space Res., 15(8/9)*, 375–384, doi:10.1016/0273-1177(94)00120-P

Kallenrode, M.-B. (1996), A statistical survey of 5-MeV proton events at transient interplanetary shocks, *J. Geophys. Res., 101*, 24409–24410, doi:10.1029/96JA01897

Krauss-Varban, D., D. Burgess, and C. S. Wu (1989), Electron acceleration at nearly perpendicular collisionless shocks. I - One-dimensional simulations without electron scale fluctuations, *J. Geophys. Res., 94*, 15089–15098, doi:10.1029/JA094iA11p15089

Krauss-Varban, D., and D. Burgess (1991), Electron acceleration at nearly perpendicular collisionless shocks. II - Reflection at curved shocks, *J. Geophys. Res., 96*, 143–154,

doi:10.1029/90JA01728

Lario, D., G. C. Ho, R. B. Decker, E. C. Roelof, M. I. Desai, and C. W. Smith (2003), ACE observations of energetic particles associated with transient interplanetary shocks, in *Solar Wind Ten, AIP Conf. Proc. Ser.*, vol. 679, edited by M. Velli, R. Bruno, F. Malara, and B. Bucci, pp. 640–643, doi:10.1063/1.1618676

Lario, D., Q. Hu, G. C. Ho, R. B. Decker, E. C. Roelof, and C. W. Smith (2005), Statistical properties of fast forward transient interplanetary shocks and associated energetic particle events: ACE observations, in *Proc. Solar Wind 11/SOHO 16, Connecting Sun and Heliosphere, ESA Special Publication*, vol. 592, edited by B. Fleck, T. H. Zurbuchen, and H. Lacoste, pp. 421–426, ESA Publications Division, Noordwijk

Mann, G., A. Klassen, H. Aurass, H., and H.-T. Classen (2003), Formation and development of shock waves in the solar corona and the near-Sun interplanetary space, *Astron. Astrophys., 400*, 329–336, doi:10.1051/0004-6361:20021593

Meyer, J., G. Wibberenz, and M.-B. Kallenrode (1993), Time-development of proton energy spectra in solar energetic particle events, *Adv. Space Res., 13(9)*, 363–366, doi:10.1016/0273-1177(93)90506-7

Michalek, G., N. Gopalswamy, and H. Xie (2007), Width of radio-loud and radio-quiet CMEs, *Sol. Phys., 246*, 409–414, doi:10.1007/s11207-007-9062-y

Nelson, G. J., & Melrose, D. B. 1985, Type II bursts, in *Solar Radiophysics: Studies of emission from the sun at metre wavelengths*, edited by D. J. McLean and N. R. Labrum, pp. 333–359, Cambridge University Press, Cambridge

Neugebauer, M., and J. Giacalone (2005), Multispacecraft observations of interplanetary shocks: Nonplanarity and energetic particles, *J. Geophys. Res., 110*, A12106,

doi:10.1029/2005JA011380

Neugebauer, M., J. Giacalone, E. Chollet and D. Lario (2006), Variability of low-energy ion flux profiles on interplanetary shock fronts, *J. Geophys. Res., 111*, A12107, doi:10.1029/2006JA011832

Sarris, E. T., and J. A. Van Allen (1974), Effects of interplanetary shock waves on energetic charged particles, *J. Geophys. Res., 79*, 4157–4173, doi:10.1029/JA079i028p04157

Sarris, E. T., G. C. Anagnostopoulos, and P. C. Trochoutsos (1984), On the E-W asymmetry and the generation of ESP events, *Sol. Phys., 93*, 195–210, doi:10.1007/BF00156665

Sarris, E. T., R. B. Decker, and S. M. Krimigis (1985), Deep space observations of the east-west asymmetry of solar energetic storm particle events - Voyagers 1 and 2, *J. Geophys. Res., 90*, 3961-3965, doi:10.1029/JA090iA05p03961

Torsti, J., E. Valtonen, M. Lumme, P. Peltonen, T. Eronen, M. Louhola, E. Riihonen, G. Schultz, M. Teittinen, K. Ahola, C. Holmlund, V. Kelhä, K. Leppälä, P. Ruuska, and E. Strömmer (1995), Energetic Particle Experiment ERNE, *Sol. Phys., 162*, 505–531, doi:10.1007/BF00733438

Tsurutani, B. T., and R. P. Lin (1985), Acceleration of greater than 47 keV ions and greater than 2 keV electrons by interplanetary shocks at 1 AU, *J. Geophys. Res., 90*, 1–11, doi:10.1029/JA090iA01p00001

van Nes, P., R. Reinhard, T. R. Sanderson, and K.-P. Wenzel (1984), The energy spectrum of 35- to 1600-keV protons associated with interplanetary shocks, *J. Geophys. Res., 89*, 2122–2132, doi:10.1029/JA089iA04p02122

Webb, G. M., G. P. Zank, C. M. Co, and D. J. Donohue (1995), Multidimensional Green's functions and the statistics of diffusive shock acceleration, *Astrophys. J., 453*, 178–206,

doi:10.1086/176379

Yashiro, S., N. Gopalswamy, G. Michalek, G., O. C. St. Cyr, S. P. Plunkett, N. B. Rich, and R. A. Howard (2004), A catalog of white light coronal mass ejections observed by the SOHO spacecraft, *J. Geophys. Res., 109*, A07105, doi:10.1029/2003JA010282

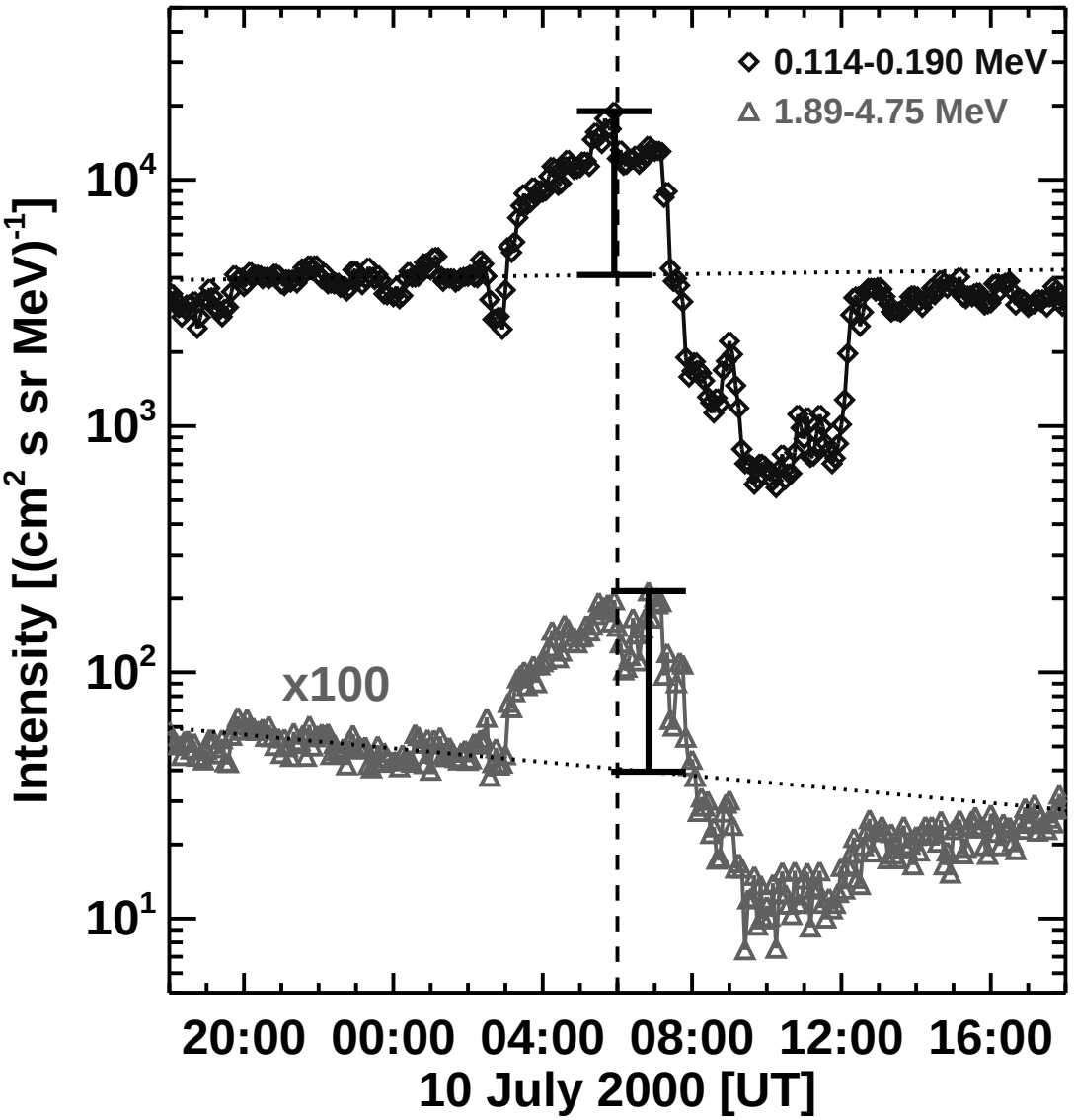

Figure 1. An example of the ESP event size estimation during the 10 July 2000 shock using ACE/EPAM 0.114–0.190 MeV (upper curve) and 1.89–4.75 MeV (lower curve) data. Dashed vertical line marks the shock and solid line the estimated increase. Dotted line shows the estimated intensity level before the ESP event. The ESP event onset is seen $\sim$ 3 hours before the shock arrival and event peaks (solid vertical lines) near the shock time.

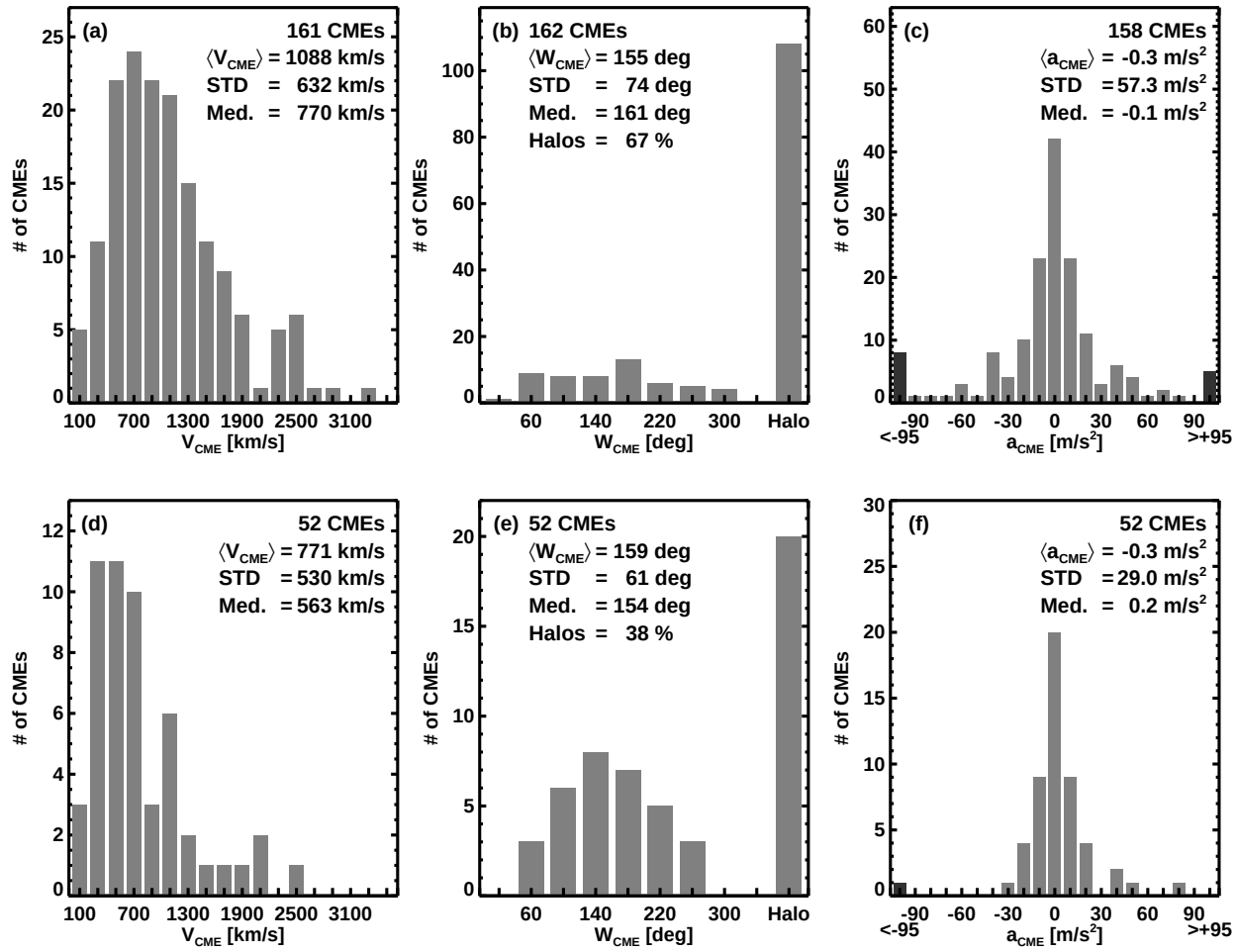

Figure 2. The speed (V_{CME}), width (W_{CME}) and acceleration (a_{CME}) distributions of the shock-driving CMEs with (top row) and without (bottom row) an ESP event. The total number of CMEs together with the average, standard deviation (STD) and median (Med.) values of the distributions are given in each panel. The CME width values given in the middle panels (b) and (e) exclude halo CMEs as their widths are unknown. The fraction of halo CMEs (Halos) is given as a percentage. The outermost dark bars of the acceleration distribution in the panels (c) and (f) include all CMEs with $a_{CME} < -95$ m/s^2 and $a_{CME} > +95$ m/s^2, respectively.

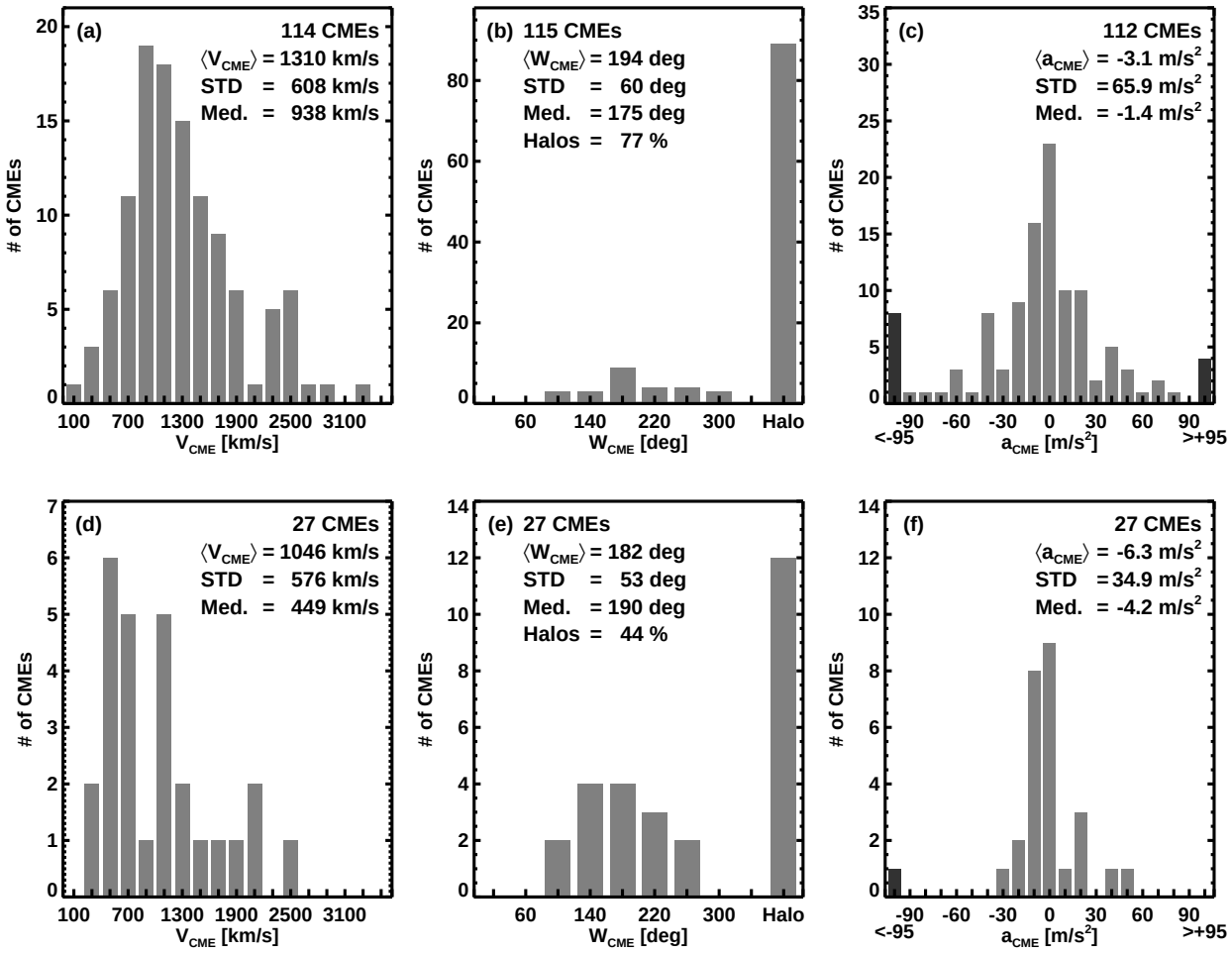

Figure 3. The distribution plots for CMEs driving RL shocks with (top row) and without (bottom row) an ESP event. The panels are as in Figure 2.

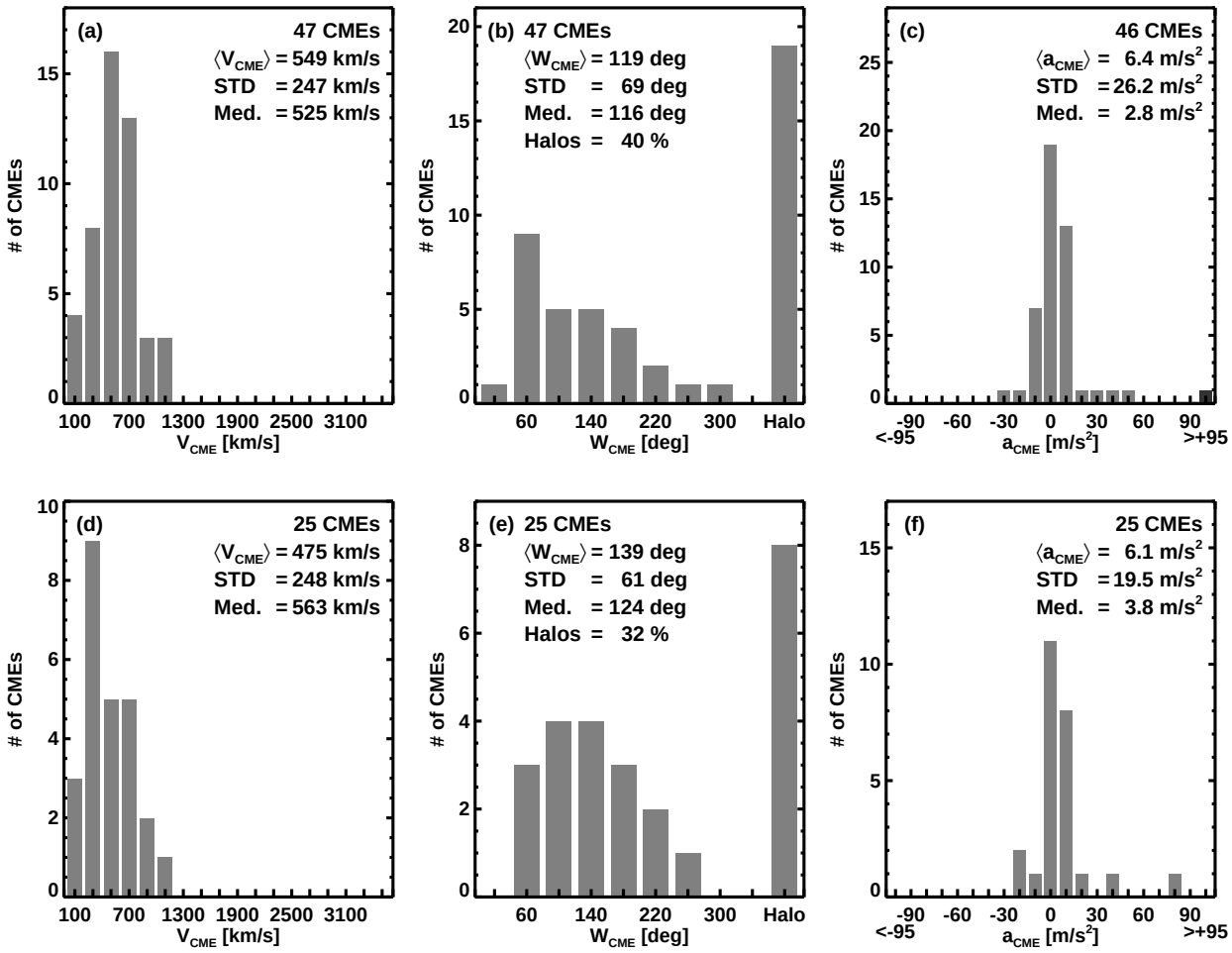

Figure 4. The distribution plots for CMEs driving RQ shocks with (top row) and without (bottom row) an ESP event. The panels are as in Figure 2.

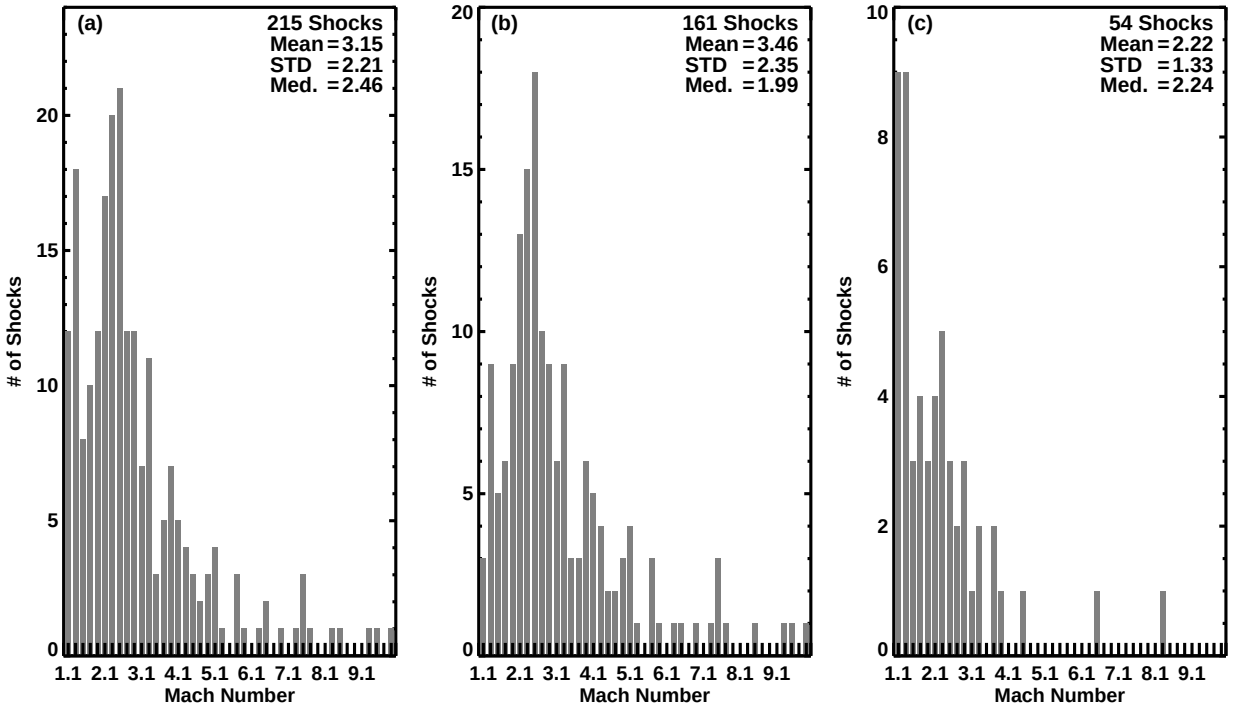

Figure 5. Distributions of shock Mach number at 1 AU for all (a), ESP-associated (b) and non-ESP associated shocks (c). The number of the shocks together with mean, standard deviation and median values are given in the plots.

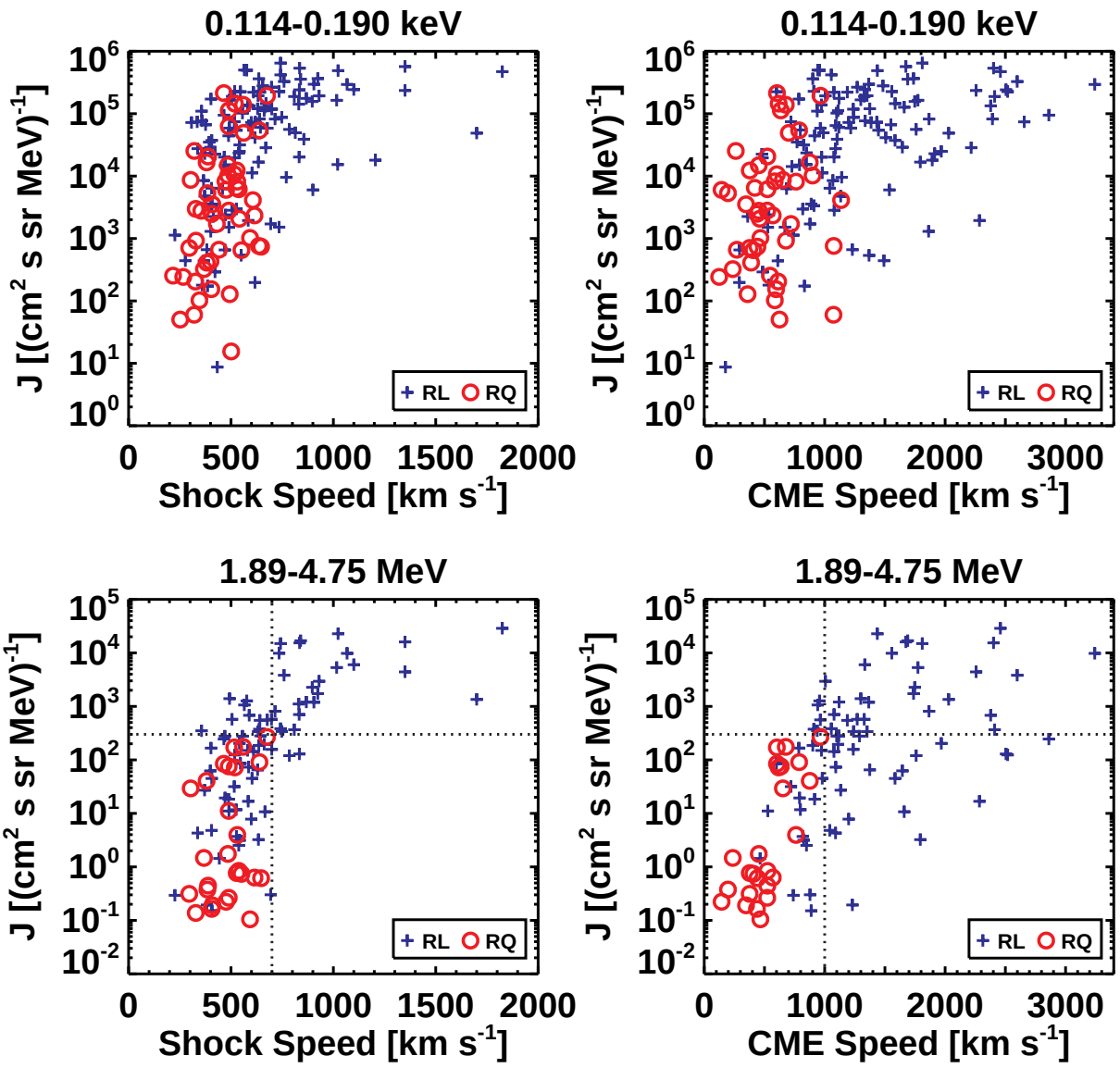

Figure 6. The ESP event size at RQ and RL shocks as a function of the shock speed (left) and CME speed (right). The ESP increases associated with the RL shocks are plotted with a plus sign and those with the RQ shocks with an open circle. Note that the RL shocks occupy the upper right portion of the plot in all cases. The dotted lines serve to guide the eye.

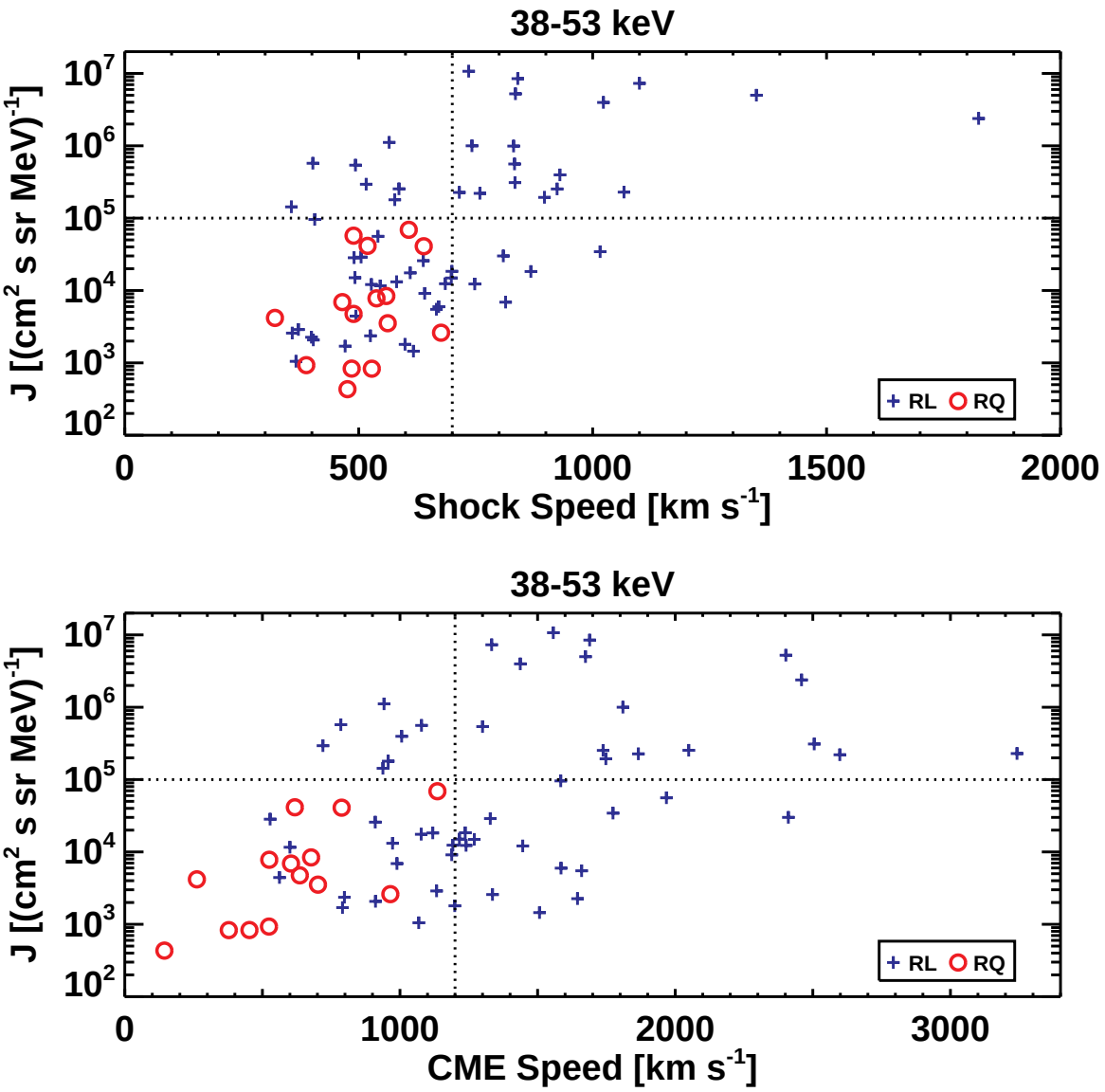

Figure 7. The size of electron enhancements at RQ (red circle) and RL (blue plus sign) shocks as a function of shock speed (top) and CME speed (bottom). The dotted lines are plotted to emphasize that all data points for the RQ event are located in the lower-left corner of the plot.

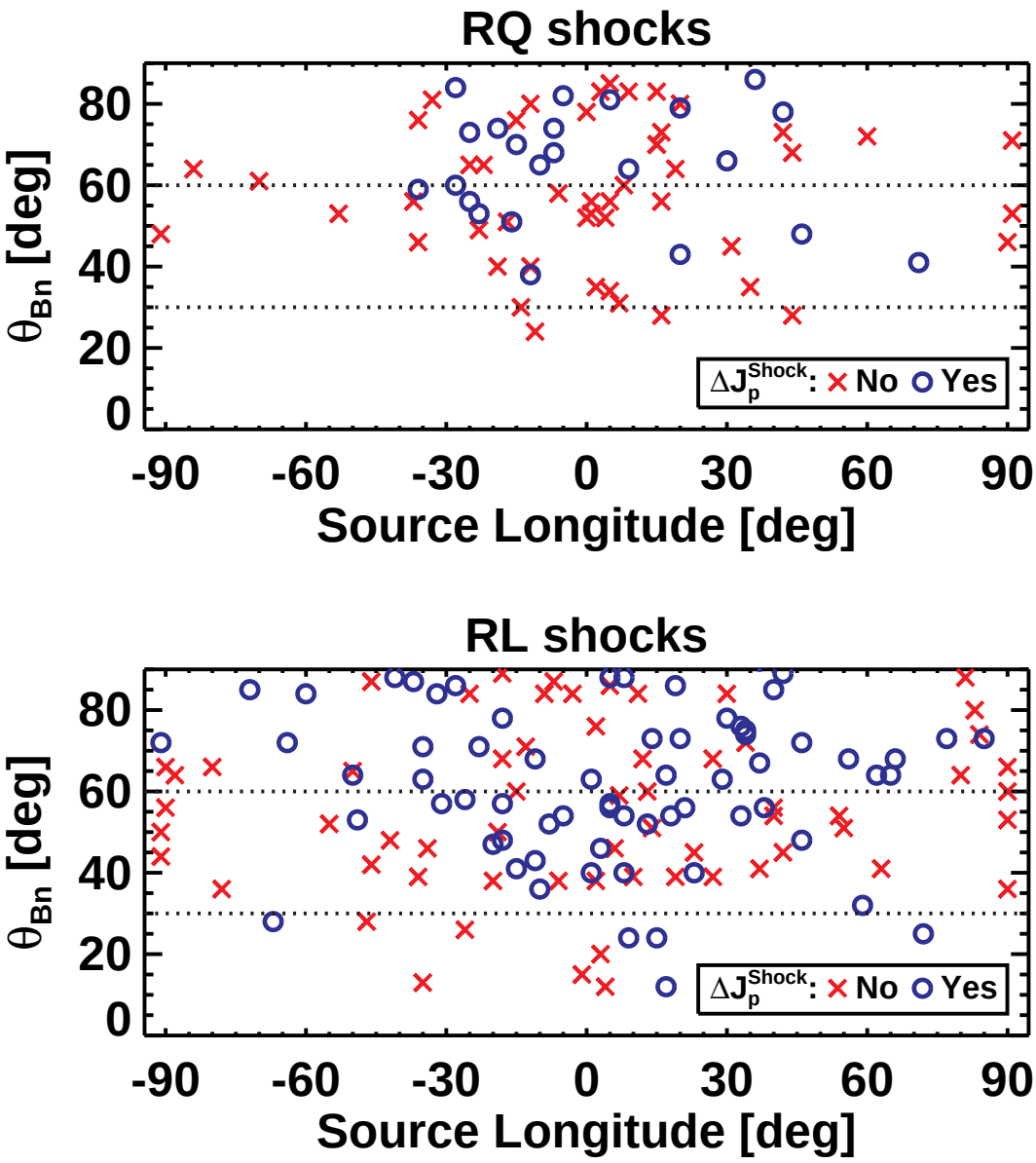

Figure 8. The shock normal angle of RQ and RL shocks as a function of source longitude. The ESP events shown were observed in the MeV energy range. Shocks originating behind the limb have been assigned a longitude of 91°. Blue circles (red crosses) mark shocks with (without) an ESP event, and the dotted lines are drawn at 30° and 60°.

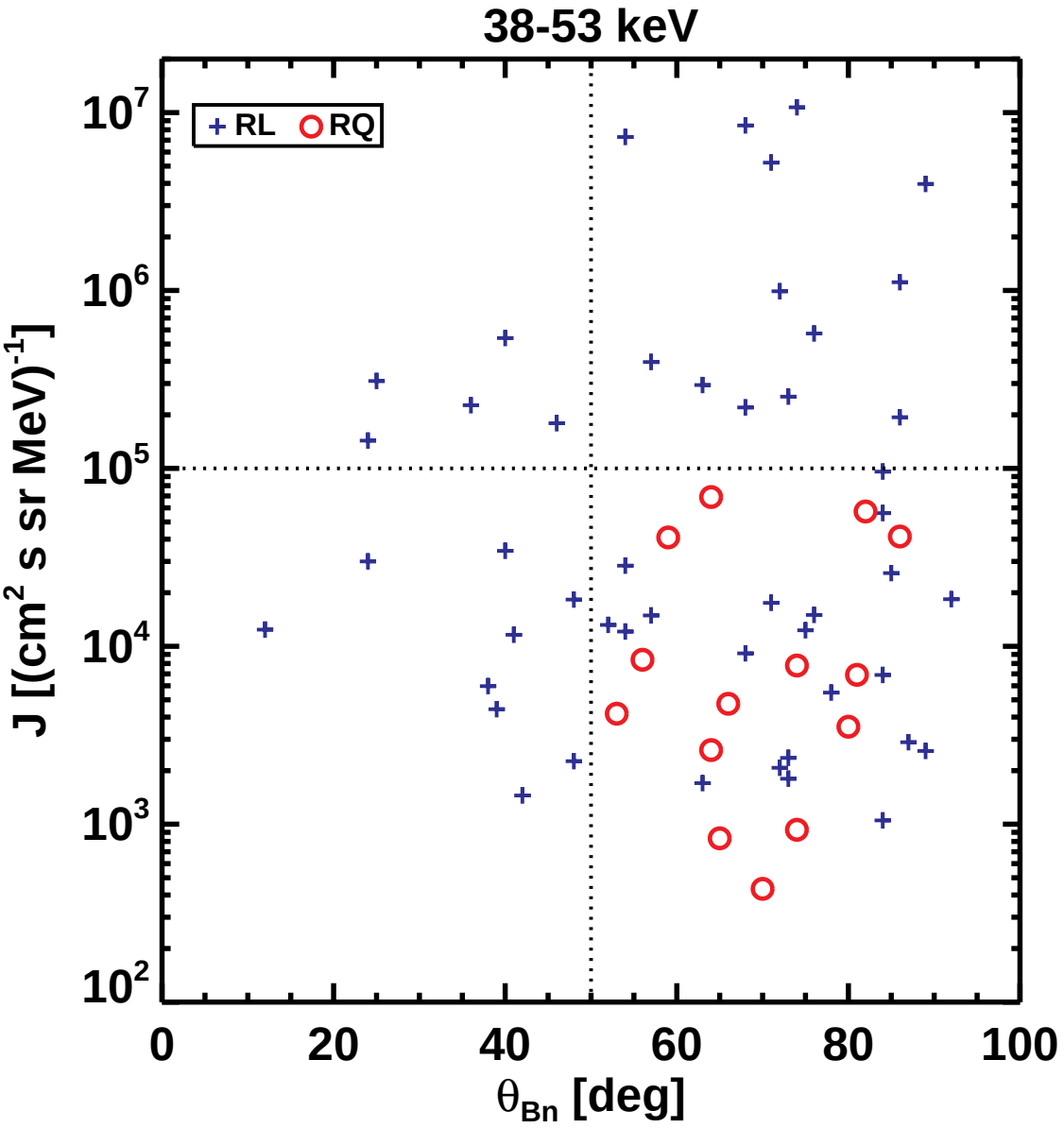

Figure 9. The size of electron enhancements at RQ (red circle) and RL (blue plus sign) shocks as a function of the shock normal angle.

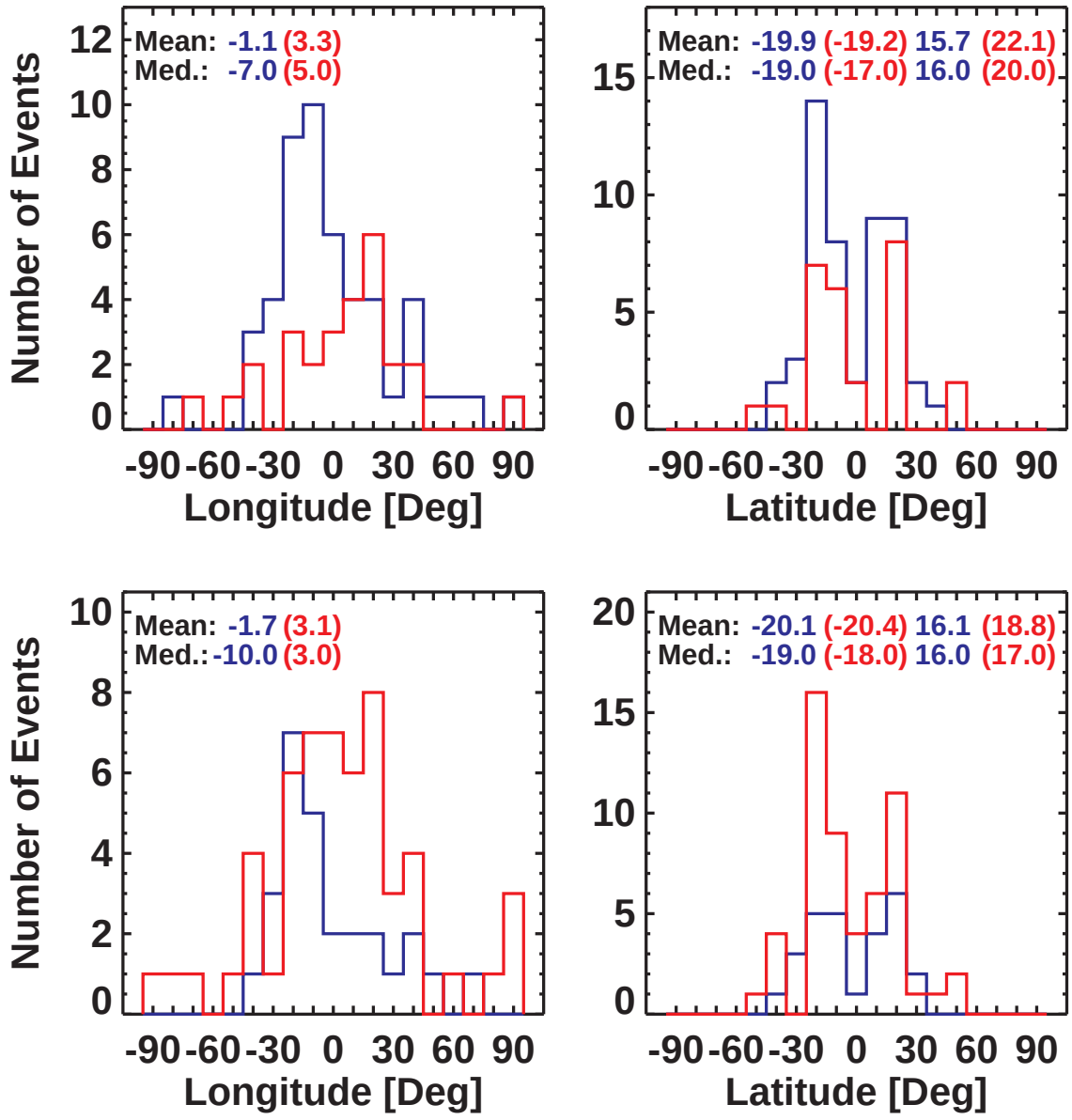

Figure 10. Distributions of source longitude (left) and latitude (right) for RQ shocks in the keV (top) and MeV (bottom) range. Blue line (red line) is for shocks with (without) an ESP event. The average and median value of source longitude and latitude for shocks with (without) an ESP event are plotted in the upper left-hand corner. For latitudes both southern (negative) and northern (positive) hemisphere mean and median values are given.

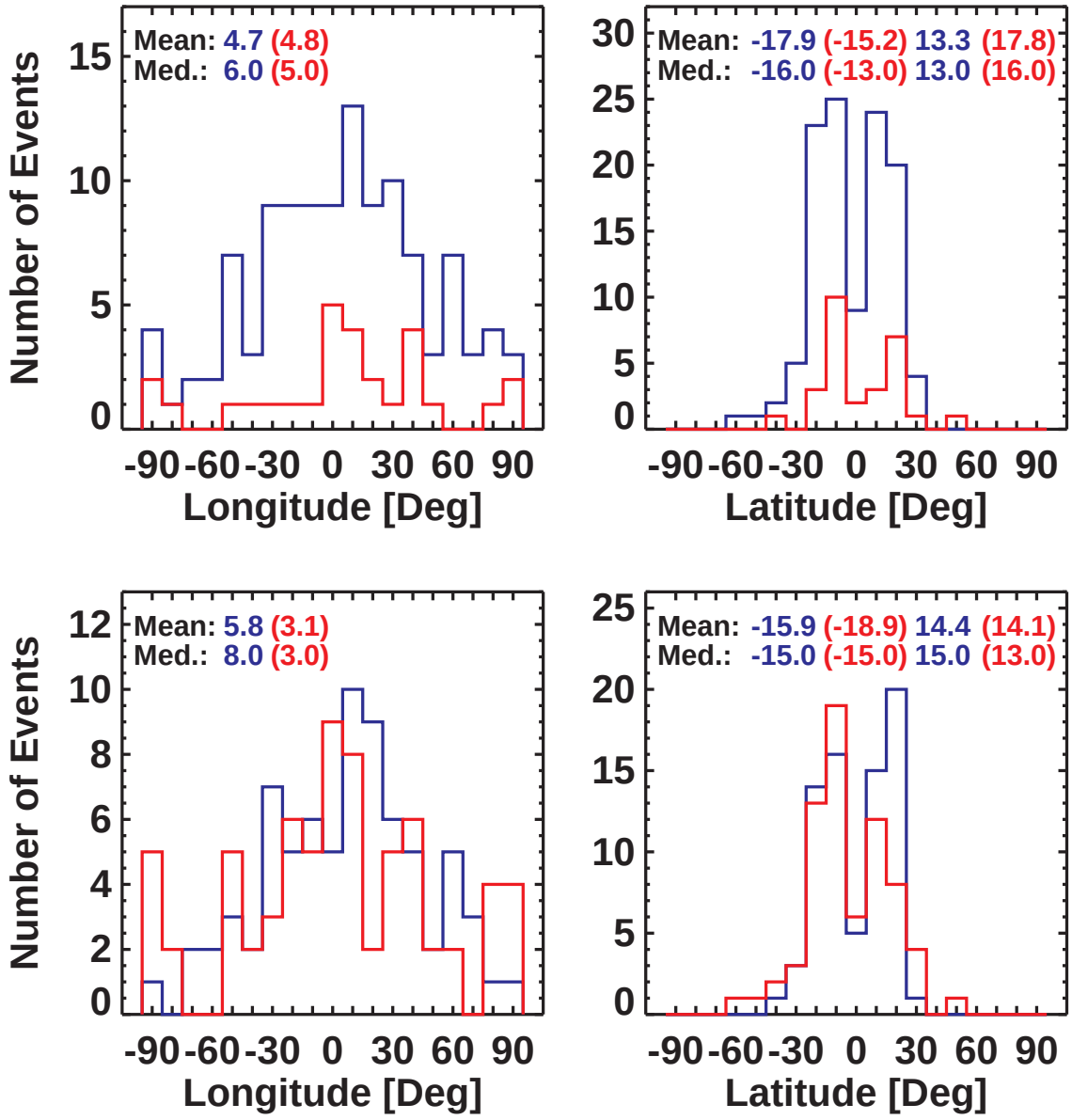

Figure 11. Distributions of source longitude (left) and latitude (right) for RL shocks in the keV (top) and MeV (bottom) range, as in Figure 10.

Table 1. Event statistics

Shock enhancements:	keV range		MeV range	
	RL	RQ	RL	RQ
ions	80%	65%	52%	32%
electrons	39%	19%	...	...
$\theta_{Bn} \geq 60°$ with shock enhancement:				
ions	53%	61%	55%	65%
$\theta_{Bn} \geq 60°$ without shock enhancement:				
ions	32%	48%	44%	48%

Table 2. Rank correlation coefficients

Energy	Shock	V_{CME}		V_{shock}	
Range	Type	ρ	$P(e)$	ρ	$P(e)$
keV:	RL	0.46	2.2e-07	0.54	3.9e-10
	RQ	0.26	7.9e-02	0.38	6.1e-03
	All	0.60	5.7e-17	0.59	7.0e-17
MeV:	RL	0.52	2.5e-06	0.68	5.1e-14
	RQ	0.76	1.1e-05	0.41	1.7e-02
	All	0.69	2.7e-15	0.70	1.6e-16